JAERI-M
9514

# BRAGG CURVE IONIZATION CHAMBER FOR PARTICLE IDENTIFICATION

June 1981

Tetsuya MURAKAMI,* Hiroshi IKEZOE, Yoshiaki TOMITA
and Naomoto SHIKAZONO

日本原子力研究所
Japan Atomic Energy Research Institute

JAERI-M 9514

# Bragg Curve Ionization Chamber for Particle Identification

Tetsuya MURAKAMI*, Hiroshi IKEZOE, Yoshiaki TOMITA
and Naomoto SHIKAZONO
Division of Physics, Tokai Research Establishment, JAERI

(Received May 12, 1981)

A Bragg curve ionization chamber was developed for particle identification, which consists of a cathode, a Frish grid and an anode. Ions entering the gas volume through the cathode are stopped between the cathode and the Frish grid. Electrons produced in the gas drift to the direction of the anode and Bragg curves of the incident ions are obtained as current signals from the anode electrode. The integral of the Bragg curve gives a total kinetic energy E and the full width of the curve corresponds to the range R. The Bragg peak value gives the atomic number. Three quantities E, R and the Bragg peak value were simultaneously measured and used for the particle identification. A resolving power $Z/\Delta Z$ of the atomic number was determined to be about 50 from the off-line data analysis of the Bragg peak value versus the range spectrum.

Keywords : Bragg Curve Ionization Chamber, Bragg Peak, Cathode, Anode, Modified Range, Particle Identification

---

* Department of Physics, Kyoto University, Kyoto 606, Japan.

JAERI－M 9514

# 荷電粒子測定用ブラッグカーブ電離箱

日本原子力研究所東海研究所物理部
村上　哲也*・池添　博・冨田　芳明・鹿園　直基

（１９８１年５月１２日受理）

ブラッグカーブ電離箱を荷電粒子識別用検出器として開発した。この検出器は，陰極，グリッド，および陽極より成り，陰極窓を通過して入射する荷電粒子を，グリッドと陰極間のガス中で止める。荷電粒子によって電離した電子は陰極・グリッド間の一様電場の中を陽極に向って移動し，入射粒子のブラッグ曲線が陽極からの電流信号として得られる。ブラッグ曲線はガス中での荷電粒子の飛跡に沿ったエネルギー損失を表わしている。このブラッグ曲線の積分値は粒子の全エネルギーになり，曲線の全幅は飛程を与える。ブラッグ曲線のピーク値は，入射荷電粒子の原子番号にのみ依存する。これら３つの量を同時に測定し，粒子識別の性能をテストした。その結果，原子番号の分解能Ｚ／△Ｚは約５０であった。

* 京都大学

Contents



目　　次

## 1. Introduction

Recently, gas detector systems are being developed for measuring the energies, atomic numbers, masses, velocities and positions of heavy-ion reaction products. They are less sensitive to the radiation damage than solid state detectors (SSD), and they can be built in a large size and have good uniformity and variability in counter thickness. Among them, a gas ionization chamber is most popular to use for the detection of heavy ions, because of its good energy resolusion and easy operation. Timing properties of a gas ionization chamber, however, are poor, and so the combination of the ionization chamber as a $\Delta E$ detector and a SSD as an E counter is often used for mass spectroscopy by the time-of-flight (TOF) method.[1] Although it is possible to identify the atomic and mass numbers of heavy ions by a counter telescope of this type, use of the SSD limits the solid angle of the telescope. Moreover a SSD is so easily damaged by the radiation effect that this system is expensive. In order to obtain a time resolusion better than 200 ps, a secondary electron detector using a microchannel plate[2] or a parallel plate avalanche counter (PPAC)[3] is frequently used. The gas counter system consisting of an ionization chamber for the energy and energy-loss measurements and the PPAC for timing is economical.[4]

For the JAERI TOF spectrometer[5] we planed to make a new type gas counter system consisting of a Bragg curve ionization chamber[6] for measuring the Bragg curves of heavy ions in the counter. From the Bragg curves the ranges R and energies E of

the incident particles are determined. The specific ionization at the Bragg curve peak $(\Delta E)_{max}$ determines the atomic number and the atomic number is easily obtained with an on-line data taking system. If a precise Bragg curve can be obtained, the mass number of heavy ions may be determined from the analysis of its shape.

We report in this paper the performance of the Bragg counter, which was investigated using $\alpha$ particles from $^{241}Am$ and $^{35}Cl$ beams from the JAERI 20 MV tandem accelerator.

## 2. Technical details of Bragg counter

### 2.1 Principle and construction

Like an ordinary gas ionization chamber, the Bragg counter consists of an anode, a Frish grid and a cathode. The distance between the cathode and the Frish grid is designed to be longer than the range of the particles to be detected. The reaction products enter the counter normal to the cathode and parallel to the electric field between the cathode and the Frish grid, and lose their kinetic energies by producing the electron-ion pairs. The electrons along the track drift to the anode through the Frish grid and are detected as an anode current. As the drift velocity of electrons is constant, it is clear that the anode current as a function of time is proportional to the specific energy loss of the particle as a function of position; i.e., the Bragg curve of the particle. The integral of the anode current corresponds to a total number of electrons and thus is proportional to the total kinetic energy E. From the duration of the anode current, we can obtain a full width of the Bragg curve, which corresponds to the range R. The specific energy loss dE/dX of

the incident particles are determined. The specific ionization at the Bragg curve peak $(\Delta E)_{max}$ determines the atomic number and the atomic number is easily obtained with an on-line data taking system. If a precise Bragg curve can be obtained, the mass number of heavy ions may be determined from the analysis of its shape.

We report in this paper the performance of the Bragg counter, which was investigated using $\alpha$ particles from $^{241}Am$ and $^{35}Cl$ beams from the JAERI 20 MV tandem accelerator.

## 2. Technical details of Bragg counter

### 2.1 Principle and construction

Like an ordinary gas ionization chamber, the Bragg counter consists of an anode, a Frish grid and a cathode. The distance between the cathode and the Frish grid is designed to be longer than the range of the particles to be detected. The reaction products enter the counter normal to the cathode and parallel to the electric field between the cathode and the Frish grid, and lose their kinetic energies by producing the electron-ion pairs. The electrons along the track drift to the anode through the Frish grid and are detected as an anode current. As the drift velocity of electrons is constant, it is clear that the anode current as a function of time is proportional to the specific energy loss of the particle as a function of position; i.e., the Bragg curve of the particle. The integral of the anode current corresponds to a total number of electrons and thus is proportional to the total kinetic energy E. From the duration of the anode current, we can obtain a full width of the Bragg curve, which corresponds to the range R. The specific energy loss dE/dX of

the heavy ion is described as

$$\frac{dE}{dX} = \bar{q}^2 S_p(v), \qquad (1)$$

where $\bar{q}$ is the effective charge of the heavy ion and $S_p(v)$ the proton stopping power and v the heavy ion velocity.[7] The effective charge $\bar{q}$ depends on the atomic number and the velocity of the incident ions. The eq. (1) expresses that the specific energy loss depends only on the atomic number and the heavy ion velocity. Therefore the maximum value of the specific energy loss $(\Delta E)_{max}$ is expected to be the same among the isotopes, and we can determine the atomic number from the $(\Delta E)_{max}$.

Figure 1 shows a schematic view of the Bragg counter. Main parts of the counter are made of stainless steel to avoid the attachment of the impurity gases and parts for which high voltage is applied are insulated by TEFLON and DELRIN. The distance between the Frish grid and the anode and the distance between the Frish grid and the cathode are 0.8 and 15.4 cm, respectively. The cathode has a window of 20 mm diameter for particles to pass through. The window is made of 30 $\mu g/cm^2$ stretched polypropylene film and metalized with 25 $\mu g/cm^2$ Al.[3] The Frish grid is made of gold-plated tungsten wires of 50 $\mu m$ diameter with intervals of 1 mm. The entrance window of 20 mm diameter is a 4 $\mu m$ aluminized mylar foil, which holds more than 300 Torr gas pressure. The distance between the window and the cathode was made as short as possible. In order to avoid concentration of electric field lines the window holder was made of a glass insulator. The anode plate has a capacitance of 38 pF against the grounded counter case. In order to keep the electric field between the cathode and the Frish grid homogeneous, 14 ring electrodes are placed at intervals

of 1.03 cm between the cathode and the Frish grid. They are electrically connected each other by using a potential divider which consists of a series of 10 MΩ resistors. The inner diameter of the ring electrode is 6 cm. This value was determined in order that almost all electrons produced in gas drift to anode without loss.

## 2.2 Gas handling system

The Bragg counter was operated with a steady flow of isobutane gas at 99 Torr for detecting α particles ($E_\alpha$ = 5.486 MeV) from $^{241}Am$ and at 120 Torr for detecting the reaction products of 145 MeV $^{35}Cl$ on Al. The flow rate of isobutane gas was regulated with the thermal mass flow meter and the precise needle valve. The change of the pressure of isobutane gas, monitored by an absolute pressure meter, was better than 1 % over a time period of two days.

## 2.3 Electronics

Figure 2 shows a block diagram of the electronic circuit used. In order to obtain the Bragg curves of the incident particles, the anode current signals were preamplified with an ORTEC 142PC charge-sensitive preamplifier and differentiated with a JAERI multimode amplifier of 0.1 μs time constant. To obtain energy signals, the signals from the preamplifier were also amplified with a shaping time constant of 4 μs using a Canberra research amplifier. Bragg curve signals were digitized with a LeCroy 8 bit waveform digitizer whose sampling period was 50 ns and conversion gain was 256. The digitized data were stored on magnetic tapes for

the off-line analysis. The Bragg curve peak and the full width of the Bragg curve signal were measured by means of a pulse width analyzer (PWA), whose electric circuit is shown in Fig.3. The PWA consists of a high speed comparator and pulse shaping elements. This module gives a pair of fast negative timing signals when the input pulse crosses a discriminating level of 200 mV. Two signals, one is leading edge timing pulse and the other is trailing edge one, are put into a time-to-amplitude converter (TAC) as start and stop pulses, respectively. The output of the TAC TAC corresponds to the pulse width; i.e., the range R of the incident particle. The energy, the range and the Bragg curve peak were collected through a MBD-11 and processed with a PDP-11/04 and 11/55 on-line computer system and stored on magnetic tapes.

## 3. Results

### 3.1 Basic characteristics of Bragg counter

Before making a large Bragg counter, a small test counter was made in order to test the basic characteristics. The size of the test counter is about one third of the large one. The test counter was operated with isobutane gas of 219, 267 and 315 Torr. The resolusions of E, R and $(\Delta E)_{max}$ were measured as functions of reduced electric field $\varepsilon_{C-G}/P$ between the cathode and the Frish grid, where P is the pressure of isobutane gas. In this measurements $\alpha$ particles from $^{241}Am$ mounted near the entrance window were collimated by a defining slit of 2 mm diameter.

In order to see the effect of trapping of electrons by the Frish grid, the pulse height of the E signal was measured as a function of $\varepsilon_{G-A}/\varepsilon_{C-G}$ value keeping the $\varepsilon_{C-G}/P$ value constant. The $\varepsilon_{G-A}$ is the electric field between the Frish grid and the anode.

the off-line analysis. The Bragg curve peak and the full width of the Bragg curve signal were measured by means of a pulse width analyzer (PWA), whose electric circuit is shown in Fig.3. The PWA consists of a high speed comparator and pulse shaping elements. This module gives a pair of fast negative timing signals when the input pulse crosses a discriminating level of 200 mV. Two signals, one is leading edge timing pulse and the other is trailing edge one, are put into a time-to-amplitude converter (TAC) as start and stop pulses, respectively. The output of the TAC corresponds to the pulse width; i.e., the range R of the incident particle. The energy, the range and the Bragg curve peak were collected through a MBD-11 and processed with a PDP-11/04 and 11/55 on-line computer system and stored on magnetic tapes.

## 3. Results

### 3.1 Basic characteristics of Bragg counter

Before making a large Bragg counter, a small test counter was made in order to test the basic characteristics. The size of the test counter is about one third of the large one. The test counter was operated with isobutane gas of 219, 267 and 315 Torr. The resolusions of E, R and $(\Delta E)_{max}$ were measured as functions of reduced electric field $\varepsilon_{C-G}/P$ between the cathode and the Frish grid, where P is the pressure of isobutane gas. In this measurements $\alpha$ particles from $^{241}Am$ mounted near the entrance window were collimated by a defining slit of 2 mm diameter.

In order to see the effect of trapping of electrons by the Frish grid, the pulse height of the E signal was measured as a function of $\varepsilon_{G-A}/\varepsilon_{C-G}$ value keeping the $\varepsilon_{C-G}/P$ value constant. The $\varepsilon_{G-A}$ is the electric field between the Frish grid and the anode.

As shown in Fig.4, as the $\varepsilon_{G-A}/\varepsilon_{C-G}$ ratio increases, the pulse height of the E signal increases rapidly and the energy resolusion $\delta E/E$ becomes better. The pulse height and the resolusion of the E signal almost saturate in the region where the value $\varepsilon_{G-A}/\varepsilon_{C-G}$ is larger than the calculated value for which all of the field lines from the cathode terminate on the anode.[8] This value is indicated by an arrow in Fig.4.

The resolusion of E, R and $(\Delta E)_{max}$ were measured as a function of $\varepsilon_{C-G}/P$, keeping the ratio $\varepsilon_{G-A}/\varepsilon_{C-G}$ constant in the saturated region. As shown in Fig.5, the resolusion of E, R and $(\Delta E)_{max}$ are almost constant in the region $\varepsilon_{C-G}/P$ >1 V/cm.Torr. In the region $\varepsilon_{C-G}/P$ <1 V/cm.Torr, however, the $(\Delta E)_{max}$ resolusion becomes worse and the pulse heights of the E and the R signals decrease rapidly as the $\varepsilon_{C-G}/P$ value decreases. Therefore the Bragg counter can be operated stably only in the region $\varepsilon_{C-G}/P$ >1 V/cm.Torr. In order to confirm the value of 1 V/cm.Torr for the large Bragg counter, the E, R and $(\Delta E)_{max}$ signals were also measured. The counter was mounted in the detector chamber of the JAERI TOF spectrometer and $\alpha$ particles from $^{241}Am$ were detected. As shown in Fig.6, almost the same value was obtained for the large Bragg counter. From these results, for the isobutane gas pressure of 120 Torr the potentials of the cathode and the Frish grid were finally chosen to be -3060 V and -360 V, respectively and the anode was grounded.

### 3.2 Particle identification

In order to investigate the particle identification capability of the Bragg counter, the elastically scattered $^{35}Cl$ ($E_{Cl}$=145 MeV)

from a Au target and the reaction products of 145 MeV $^{35}Cl$ on Al were detected at a scattering angle of 20°. The resolusion of the E, R and $(\Delta E)_{max}$ signals were 0.8 %, 1.6 % and 1.9 %, respectively for the elastically scattered $^{35}Cl$ ions. The E and R resolusions are mainly limited by the energy straggling in the entrance window of a 4 μm mylar foil and inhomogenity of the window.

Two-dimensional $(\Delta E)_{max}$ versus E, $(\Delta E)_{max}$ versus R and 1/R versus E spectra are shown in Fig.7. The reaction products from Ne to K are cleary separated. For heavier elements than K, the energy loss in the entrance window is so large that they cannot deeply enter the Bragg counter. For lighter elements than Ne, the gas pressure was not high enough to stop the particles in the drift space of the counter. Although it is expected from the eq.(1) that the $(\Delta E)_{max}$ for the same isotopes is independent of the energy of the particle; i.e., of the range R, it changes exponentially as a function of R. This fact is mainly due to a screening inefficiency of the Frish grid as pointed out by Gruhn.[9] We used a harp grid made of 50 μm wires with 1 mm wire spacing. The distance of 0.8 cm between the Frish grid and the anode is not large enough compared with the wire spacing to shield the anode against the positive ions produced in the drift space. In our case the inefficiency of shielding $\sigma$[8] is 3.6 %. Although the $(\Delta E)_{max}$ value varies as a function of R, the atomic number is roughly identified only by the $(\Delta E)_{max}$ value. This is a very usefull to identify the atomic number with an on-line data analysis.

In order to obtain the particle identification spectrum, we tried to project the $(\Delta E)_{max}$-E, $(\Delta E)_{max}$-R and R-E curves with the

empirical formula $PI_1 = (\Delta E)_{max} - A(E+a)$, $PI_2 = (\Delta E)_{max}/(1-B\times EXP(-C\times R))$ and $PI_3 = (R-D)/E$, respectively. Here $A = b\times(\Delta E)_{max}+c$ and $D = a'\times(\Delta E)_{max}+b'$. The parameters a, b, c, B, C, a' and b' were determined by the fitting procedure of respective curves. From these data analysis, the atomic number separation was excellent and the best atomic number spectrum obtained from the $(\Delta E)_{max}$ versus R spectrum is shown in Fig.8. In the figure heavier elements than Ca were suppressed by a range limitation; i.e., only the region $R > R_c$ was analyzed as shown in Fig.7. The resolusion of atomic number $\Delta Z/Z$ is about 1/50. As the range R has a dependence on the mass numbers, $PI_2$ and $PI_3$ were expected to have a mass information. However $PI_2$ and $PI_3$ showed no marks of mass splitting.

The typical digitized waveforms of the elastically scattered $^{35}Cl$ from the Au target are shown in Fig.9. In the figure dotted line corresponds to the waveform of the 129.8 MeV $^{35}Cl$ and open circle corresponds to the one of the 79 MeV $^{35}Cl$. The pulse height of the Bragg curve for the lower energy is smaller in any points of the digitized curve than the one for the higher energy. This fact may be due to the screening inefficiency of the Frish grid. Moreover there are some dips and bumps in the curve. This is ascribed to electrical noises and a space charge effect in the drift space. The electrical noises contribute to one half of the total amplitudes of these dips and bumps. Since the $\varepsilon_{C-G}$ value of 1.46 V/cm.Torr is lower than a saturated region of the electron drift velocity in the isobutane gas, the electron drift velocity is affected by local electric fields due to the space charge of the positive ions. These dips and bumps were observed also in the waveforms recorded for the reaction products of the $^{35}Cl$ on Al.

The shape analysis of the Bragg curve itself was tried in the hope that the better particle identification including the mass identification should be made independent of the time scale of the Bragg curve, if the proper parametrization was chosen. This means that, in principle, particle identification can be made irrespective of the incident angle of the particle to the Bragg counter and the slow change of the gas pressure. Several parametrization were tried. The obtained resolusion of the atomic numbers was almost the same as the one extracted from the $(\Delta E)_{max}$ versus R spectrum and the mass separation could not obtained. The reason for these rather dissapointing results could be attributed to the distortion of the Bragg curve due to the space charge effect and the insufficient conversion gain of the waveform digitizer for this purpose.

There is another possibility of separating the mass numbers by improving the range measurements. The range R of a particle with an incident energy $E_0$ is defined as follows;

$$R = \int_0^{E_0} \frac{dE}{(dE/dX)}. \tag{2}$$

To make a mass number dependence on R clear, the eq.(2) is rewritten as

$$R = \frac{1}{2} M \int_0^{2E_0/M} \frac{d(v^2)}{(dE/dX)} = M \times F(E_0/M), \tag{3}$$

where M is a nuclear mass. From the eq.(1) a function $F(E_0/M)$ depends only on the incident velocity and the atomic number. A range difference R(M+1)-R(M) can be written as

$$R(M+1)-R(M) = M[F(E_0/(M+1))-F(E_0/M)] + F(E_0/M).$$

Using the following relation

$$F(E_0/(M+1))-F(E_0/M) \simeq E_0[M(M+1)(dE/dX)_{E=E_0}]^{-1},$$

we finally obtain the mass dependence on R as follows;

$$\frac{R(M+1)-R(M)}{R(M+1)} \simeq \frac{1}{M+1}\left[1-\langle dE/dX\rangle/(dE/dX)_{E=E_0}\right], \quad (4)$$

where $\langle dE/dX\rangle$ is an average energy loss of the incident particle with the kinetic energy $E_0$ and equal to $E_0/R$. The average energy loss $\langle dE/dX\rangle$ and the energy loss $(dE/dX)_{E=E_0}$ are almost the same order in the present mass and energy regions. For instance, the ratio $\langle dE/dX\rangle/(dE/dX)_{E=E_0}$ is less than 1.3 for the 145 MeV $^{35}Cl$. Therefore a mass number dependence of the range R is weaker than the first power of M. On the other hand, a length between the peak value and the leading edge of the Bragg curve has more sensitive dependence on M. A modified range r is give by

$$r = \frac{1}{2} M \int_0^{v_p^2} \frac{d(v^2)}{(dE/dX)} = M \times C, \quad (5)$$

where $v_p$ is a velocity corresponding to the peak value and C a constant independent of M. Therefore the modified range r is proportional to M and more sensitive to the mass number than the ordinary range R. If r is measured instead of R, the mass identification will be possible.

## 4. Summary and conclusion

The characteristics of the Bragg counter for the particle identification of heavy ions have been investigated and are summarized as follows.

The energy resolusion of the Bragg counter is comparable to those obtained with the ordinary ionization chambers. The resolusion is mainly limited by the straggling in the entrance window and its inhomogenity.

we finally obtain the mass dependence on R as follows;

$$\frac{R(M+1)-R(M)}{R(M+1)} \simeq \frac{1}{M+1}\left[1-\langle dE/dX\rangle/(dE/dX)_{E=E_0}\right], \quad (4)$$

where $\langle dE/dX\rangle$ is an average energy loss of the incident particle with the kinetic energy $E_0$ and equal to $E_0/R$. The average energy loss $\langle dE/dX\rangle$ and the energy loss $(dE/dX)_{E=E_0}$ are almost the same order in the present mass and energy regions. For instance, the ratio $\langle dE/dX\rangle/(dE/dX)_{E=E_0}$ is less than 1.3 for the 145 MeV $^{35}Cl$. Therefore a mass number dependence of the range R is weaker than the first power of M. On the other hand, a length between the peak value and the leading edge of the Bragg curve has more sensitive dependence on M. A modified range r is give by

$$r = \frac{1}{2} M \int_0^{v_p^2} \frac{d(v^2)}{(dE/dX)} = M \times C, \quad (5)$$

where $v_p$ is a velocity corresponding to the peak value and C a constant independent of M. Therefore the modified range r is proportional to M and more sensitive to the mass number than the ordinary range R. If r is measured instead of R, the mass identification will be possible.

## 4. Summary and conclusion

The characteristics of the Bragg counter for the particle identification of heavy ions have been investigated and are summarized as follows.

The energy resolusion of the Bragg counter is comparable to those obtained with the ordinary ionization chambers. The resolusion is mainly limited by the straggling in the entrance window and its inhomogenity.

Separation of different elements up to Z = 50 is possible in the energy region larger than the energy at the Bragg peak. Although the mass identification was not possible in the measurements of the range R, it may be possible in lighter isotopes by measuring the modified range r.

The Bragg counter has an intrinsic advantage over the ordinary ionization chambers. The Bragg counter has a rather simple structure and is easily made. As the distance between the cathode and the anode is large, the anode capacitance becomes small and electrical noises are reduced. The cylindrical structure of the drift space produces an uniform electric field in the whole region of the drift space.

Measurable energy region is broad at a given gas pressure compared to the conventional gas ionization chamber. In the conventional gas ionization chamber there is a $\Delta E$ electrode. Therefore incident particles to be detected should have energies large enough to pass through the $\Delta E$ electrode region. On the other hand, the Bragg counter has no such a $\Delta E$ electrode and following energy region is acceptable: from energies corresponding to the Bragg peak of the incident particles up to higher energies corresponding to the maximim range of the Bragg counter.

The authors are grateful to the JAERI tandem crew for the operation of the tandem accelerator. This work was performed under the corporation research between JAERI and Kyoto University.

References

1) A.Gamp, W.Bohne, P.Braun-Munzinger and C.K.Gelbke, Nucl. Instr. and Meth. 120 (1974) 281, J.Barrette, P.Brau-Munzinger and C.K.Gelbke, Nucl. Instr. and Meth. 126 (1975) 181.

2) H.Ikezoe, G.Isoyama and N.Shikazono, JAERI-M 7800 (1978).

3) A.Shibuya and E.Takekoshi, JAERI-M 8425 (1979), K.Tsumaki, F.Fukuzawa and E.Takekoshi, JAERI-M 8884 (1980).

4) K.Kusterer,J.Betz, H.L.Harney, B.Heck, L.K.Pao and F.Porto, Nucl. Instr. and Meth. 177 (1980) 485.

5) H.Ikezoe, T.Murakami, Y.Tomita and N.Shikazono, Contribution to the INS International Conference on Radiation Detector, Tokyo, Japan, 1981.

6) C.R.Gruhn, J.Mahoney, D.K.Scott, A.C.Shotter, T.J.M.Symons, G.Wozniak, R.Devries and W.Sondheim, LBL-9711, UC-34, p 210.

7) L.C.Northcliffe and R.F.Schilling, Nucl. Data Tables, A7 (1970) 233.

8) S.C.Curran and H.W.Wilson, in Alpha-, beta- and gamma-ray spectroscopy, ed. by K.Siegbahn, North-Holland, Amsterdam, 1966, p 303.

9) C.R.Gruhn, Contribution to the INS International Conference on Radiation Detector, Tokyo, Japan, 1981.

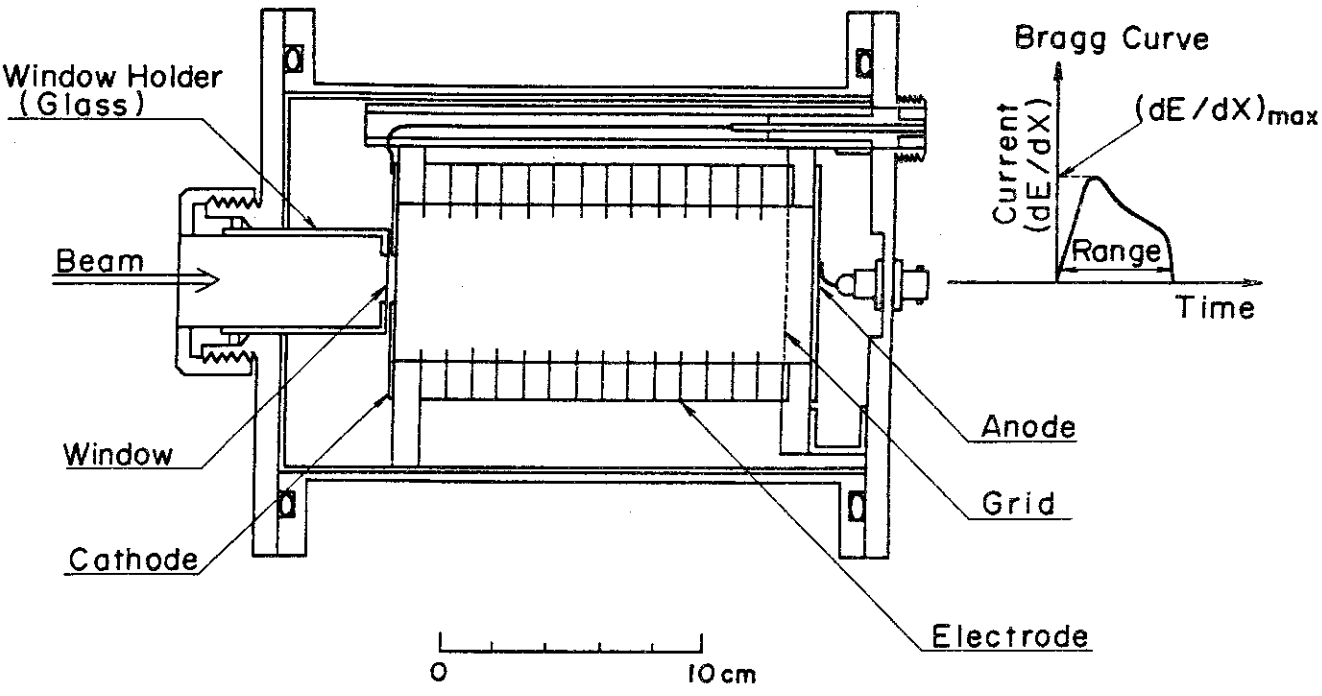


Fig.1 Schematic view of the Bragg curve ionization chamber.

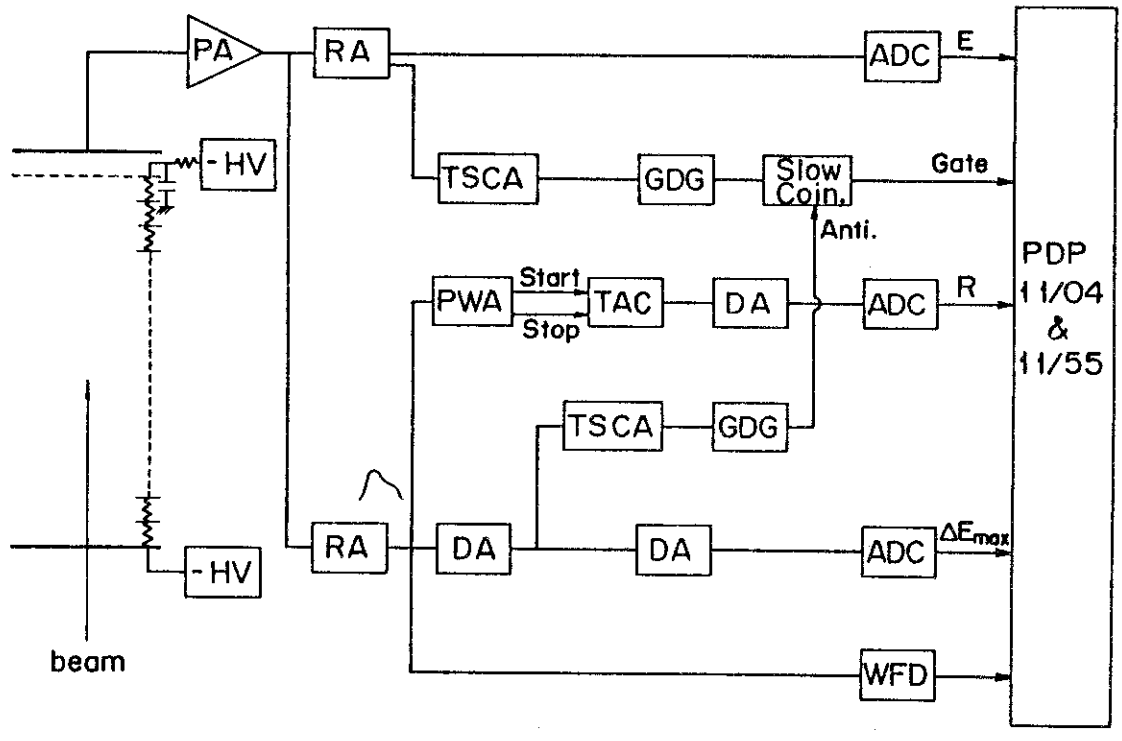


Fig.2 Block diagram of the electronic circuit. PA: charge-sensitive preamplifier. RA: research amplifier. TSCA: timing single channel analyser. DA: delay amplifier. PWA: pulse width analyser. TAC: time-to-amplitude converter. GDG: gate and delay generator. WFD: waveform digitizer.

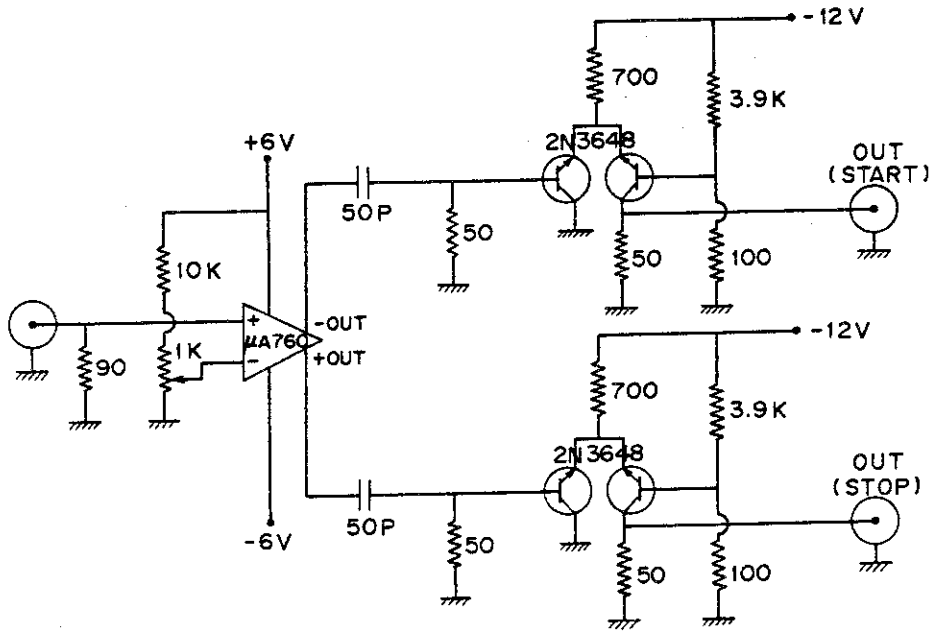


Fig.3 Schematic of the pulse width analyser (PWA).

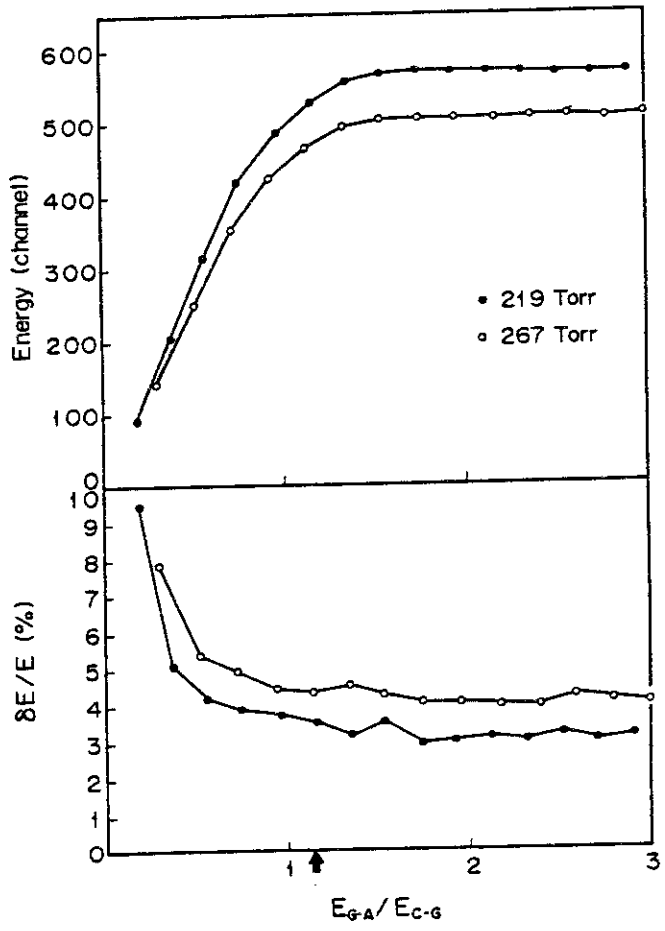


Fig.4
The Pulse height and the resolusion of the energy signal E versus the ratio $\varepsilon_{G-A}/\varepsilon_{C-G}$, where $\varepsilon_{G-A}$ and $\varepsilon_{C-G}$ are an electric field between the Frish grid and the anode and the one between the cathode and the Frish grid, respectively. Data shown obtained for the test Bragg counter using α particles from $^{241}Am$. The counter was operated with the isobutane gas of 219 and 267 Torr. An arrow shown indicates a calculated value for which all of the field lines from the cathode terminate on the anode.[8)]

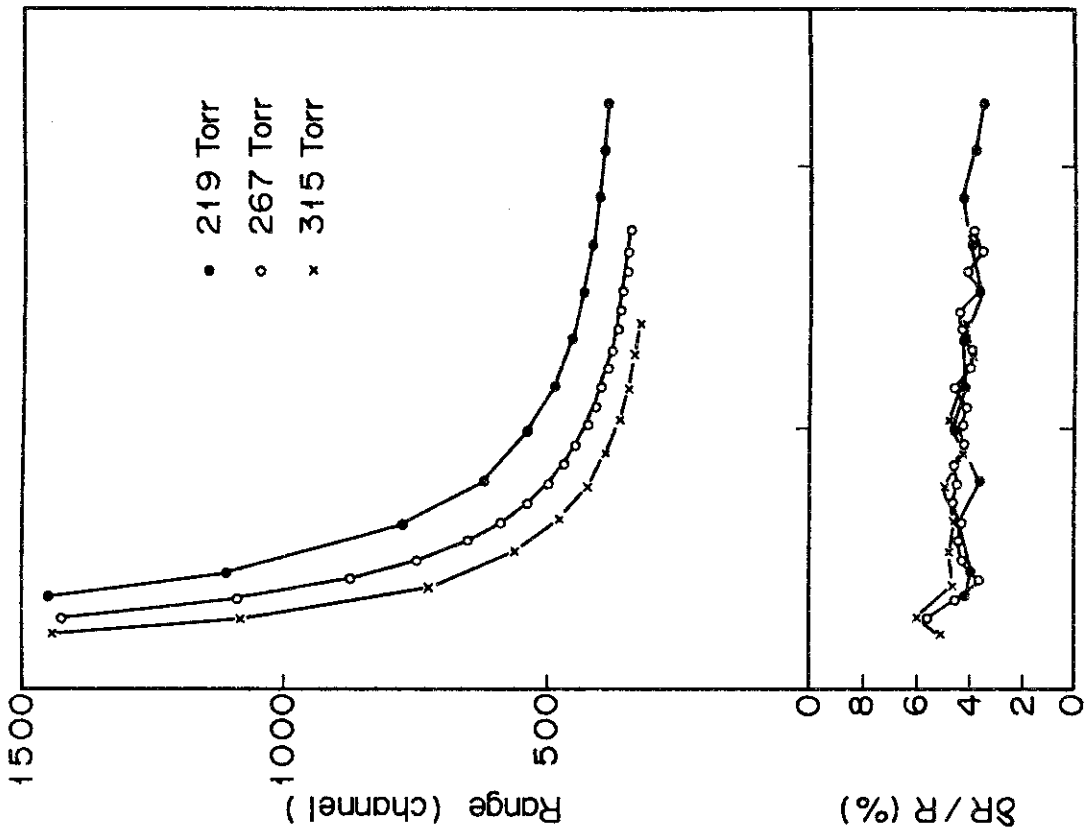


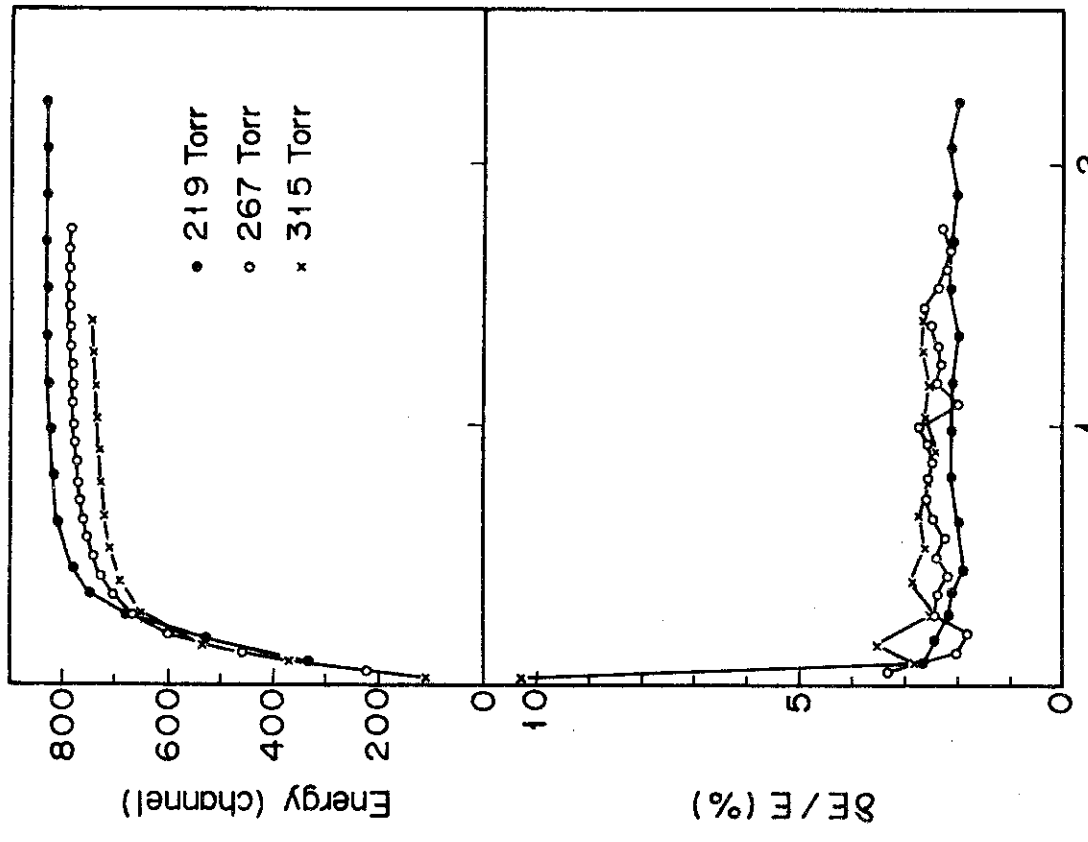


Fig. 5 Pulse height and the resolusion of **E, R and** $(\Delta E)_{max}$ **versus the** reduced electric field $\varepsilon_{C-G}/P$ for the test Bragg counter.

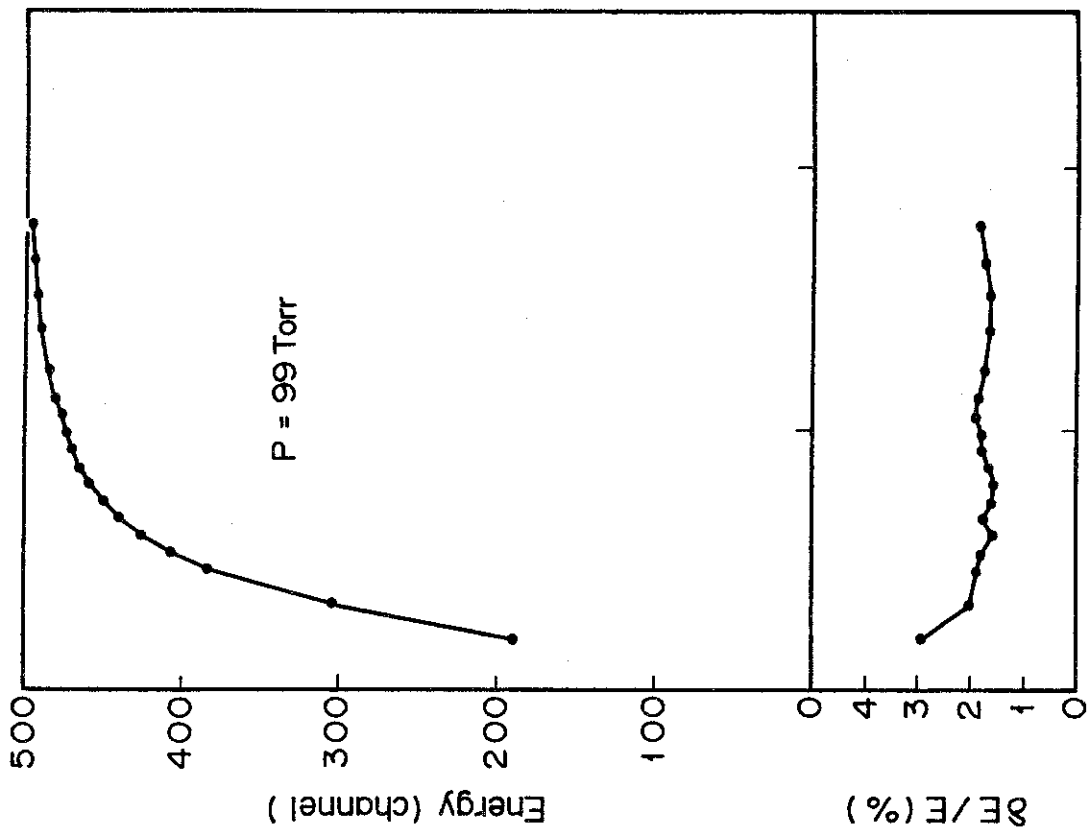


Fig. 6 Pulse height and the resolusion of E, R and $(\Delta E)_{max}$ versus the reduced electric field $\varepsilon_{C-G}/P$ for the large Bragg counter.

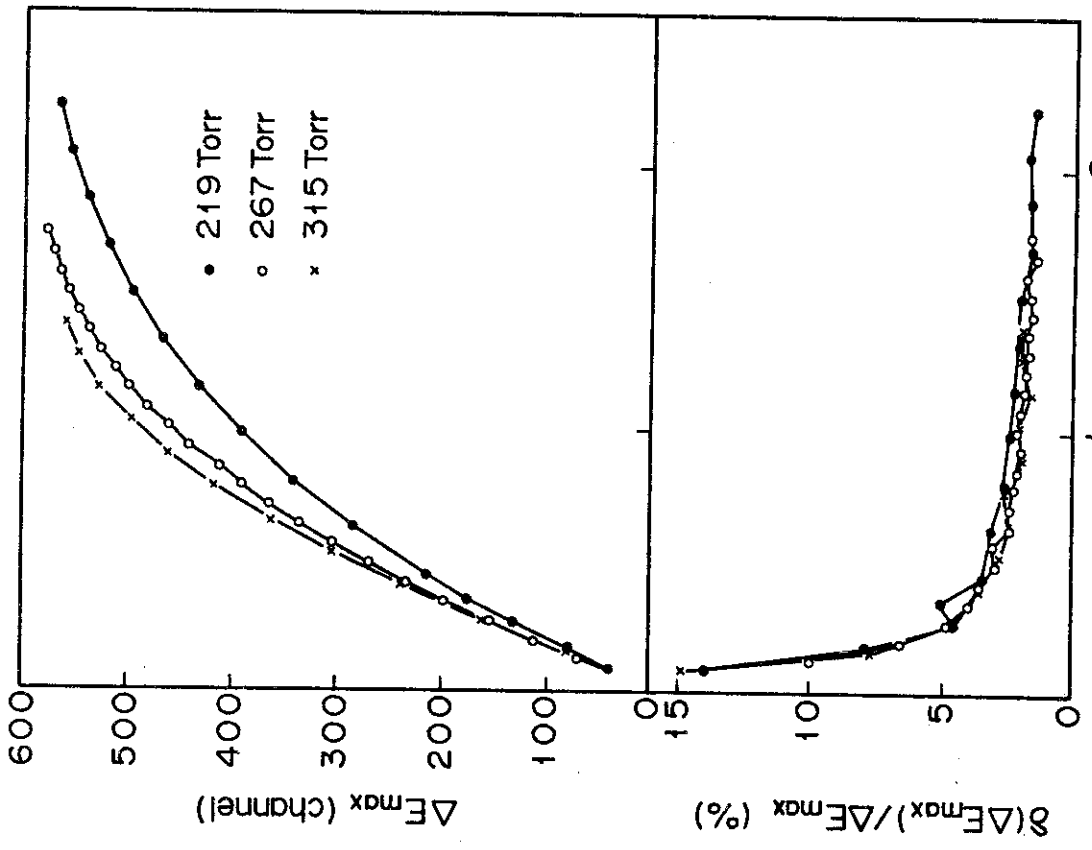


Fig.5 (c)

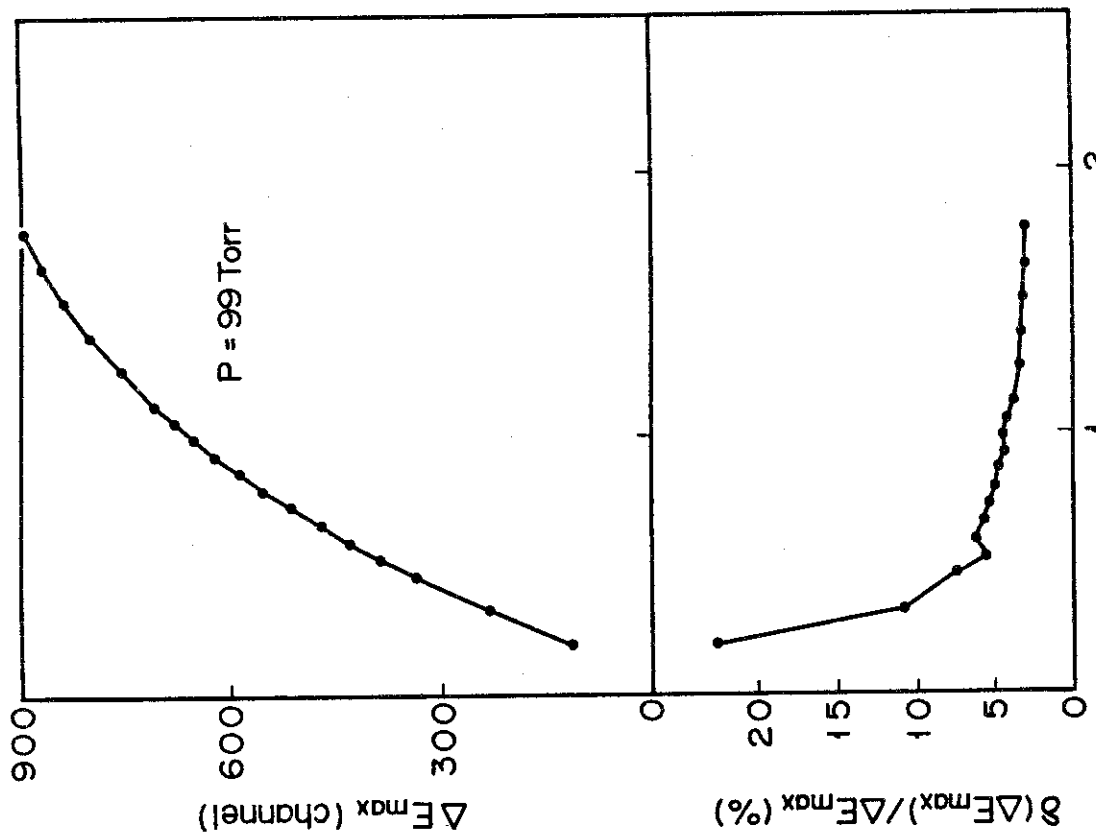
P = 99 Torr
ΔEmax (channel)
δ(ΔEmax)/ΔEmax (%)
EC-G/P (volt/(cm·Torr))

Fig.6 (c)

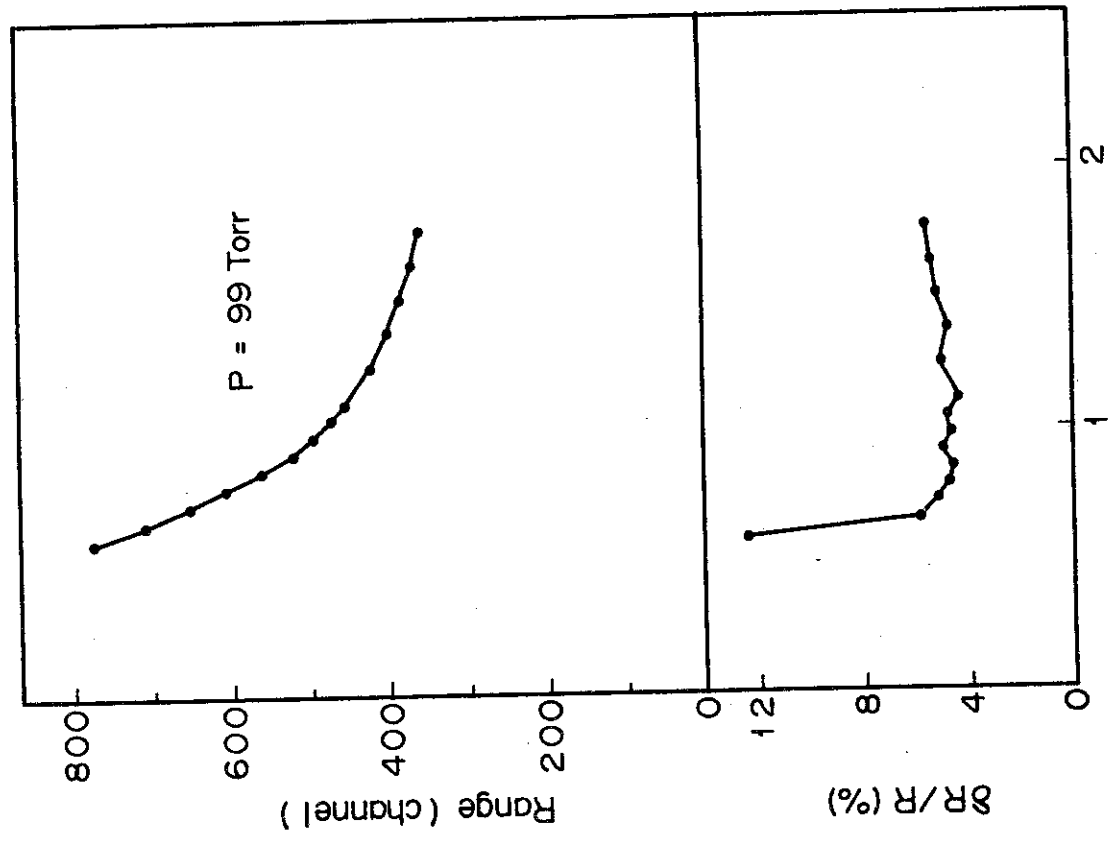
P = 99 Torr
Range (channel)
δR/R (%)
EC-G/P (volt/(cm·Torr))

Fig.6 (b)

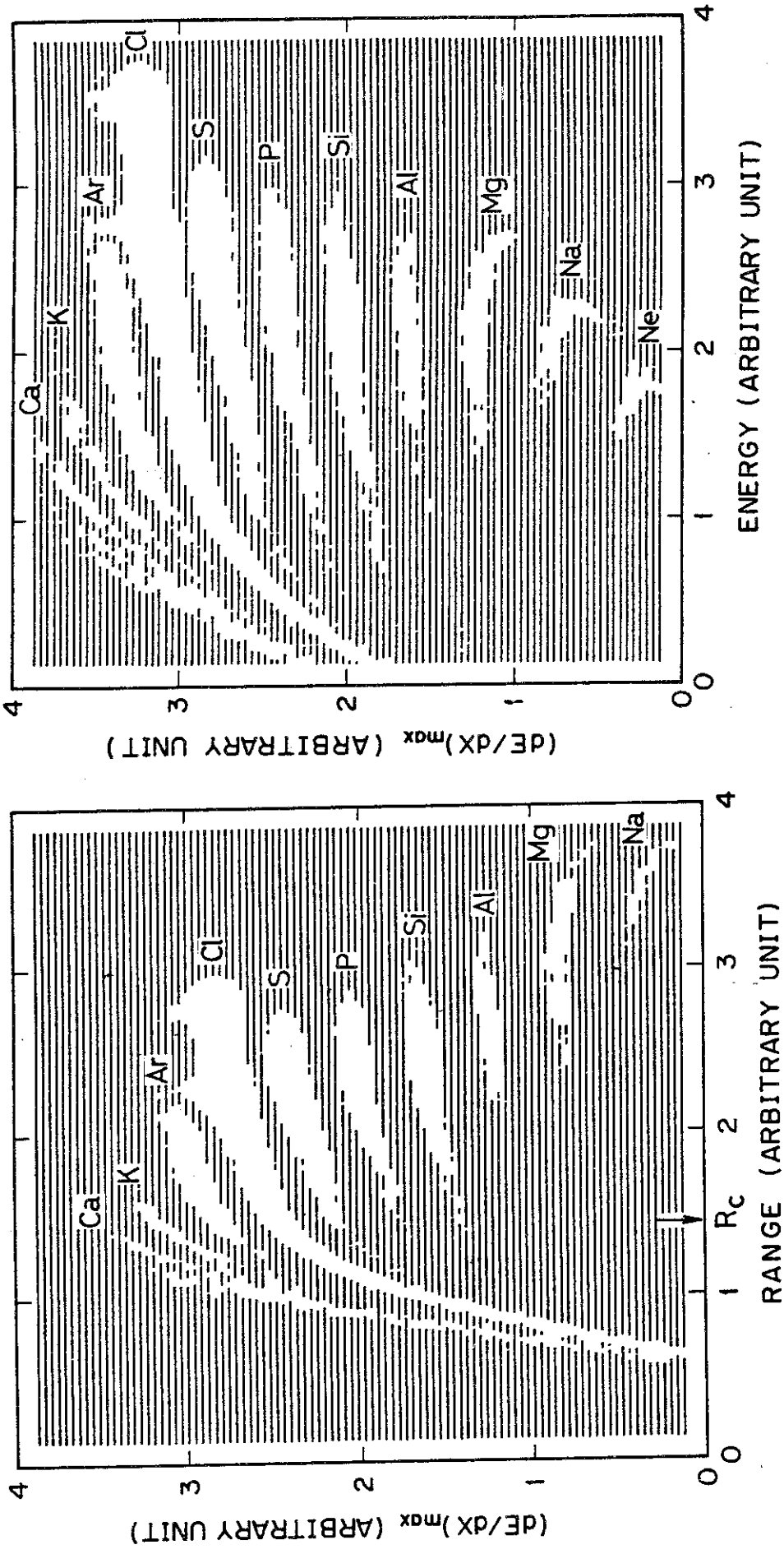


Fig. 7 Reaction products of 145 MeV $^{35}Cl$ on Al were detected by the large Bragg counter at the scattering angle of 20°.
(a): two-dimensional $(\Delta E)_{max}$ versus E spectrum. (b): two-dimensional $(\Delta E)_{max}$ versus R spectrum. A region of $R > R_c$ was analized to obtain the charge spectrum.
(c): two-dimensional 1/R versus E spectrum.

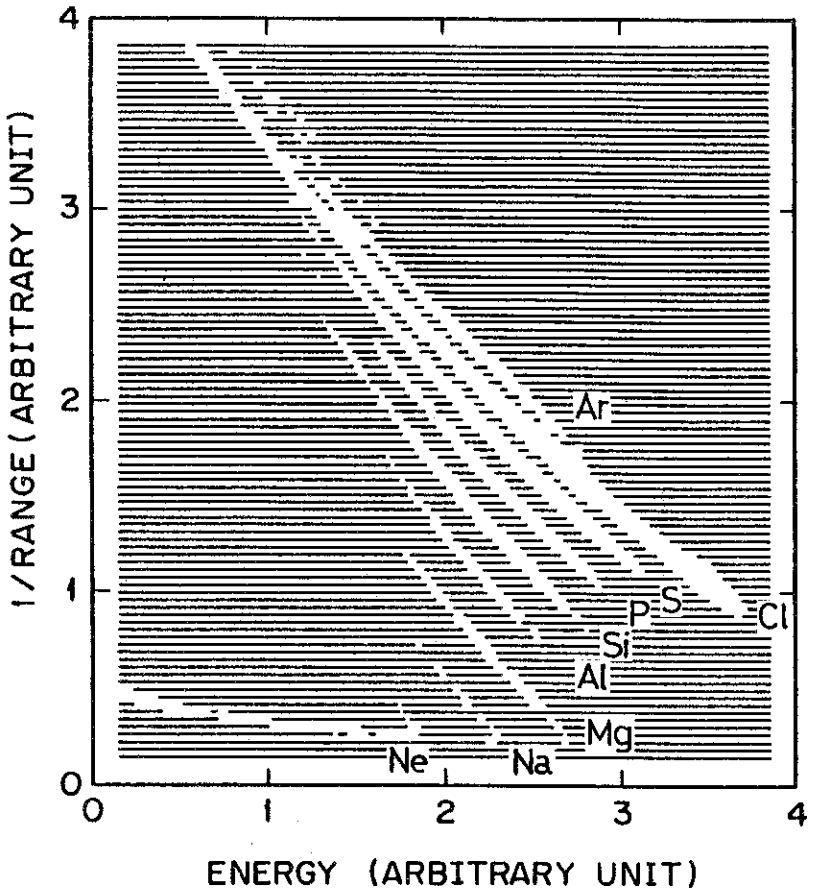


Fig.7 (c)

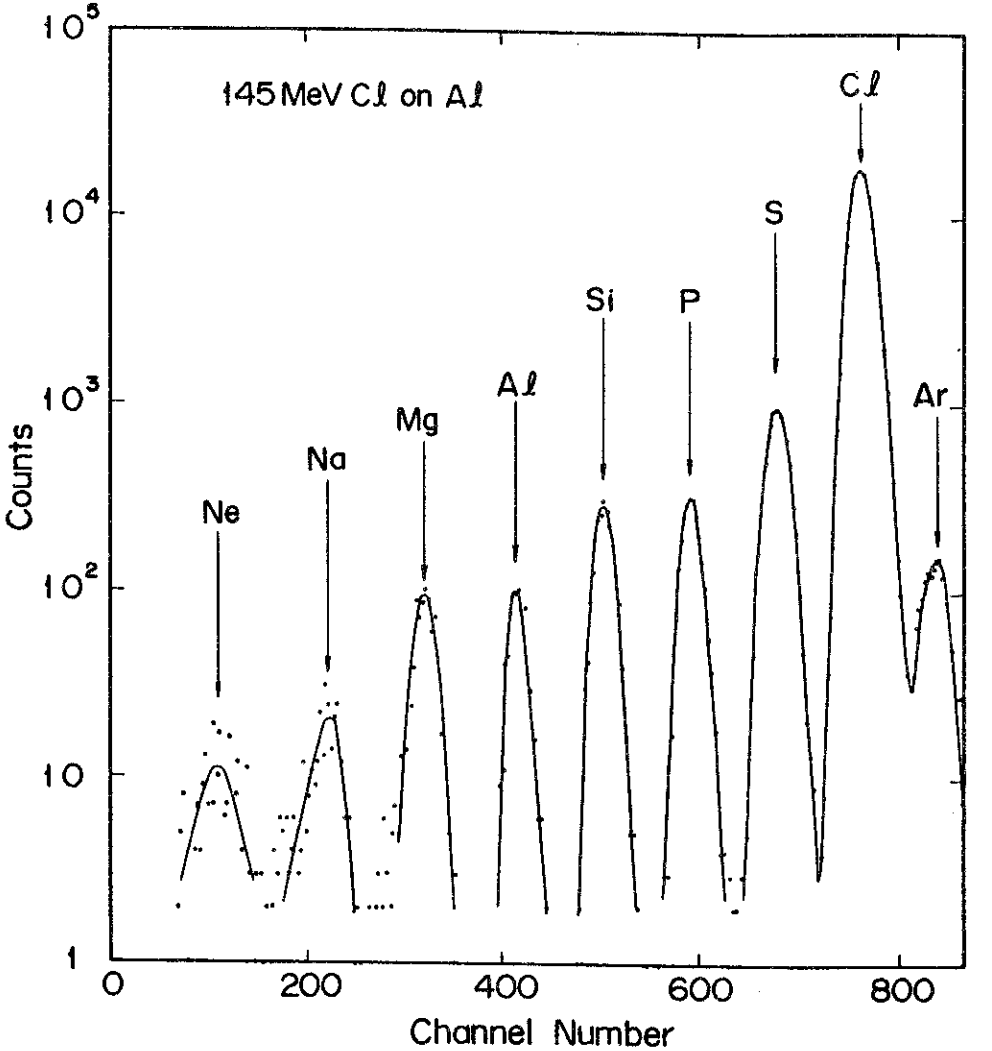


Fig.8 Charge spectrum obtained from the analysis of the $(\Delta E)_{max}$ versus R spectrum. The region $R > R_c$ shown in Fig.7(b) was analized. A particle identification function was defined as $PI_2 = (\Delta E)_{max}/(1-B\times EXP(-C\times R))$, where the parameters B and C were determined to be 60 and 0.023, respectively by the fitting procedure of the $(\Delta E)_{max}$ versus R curves.

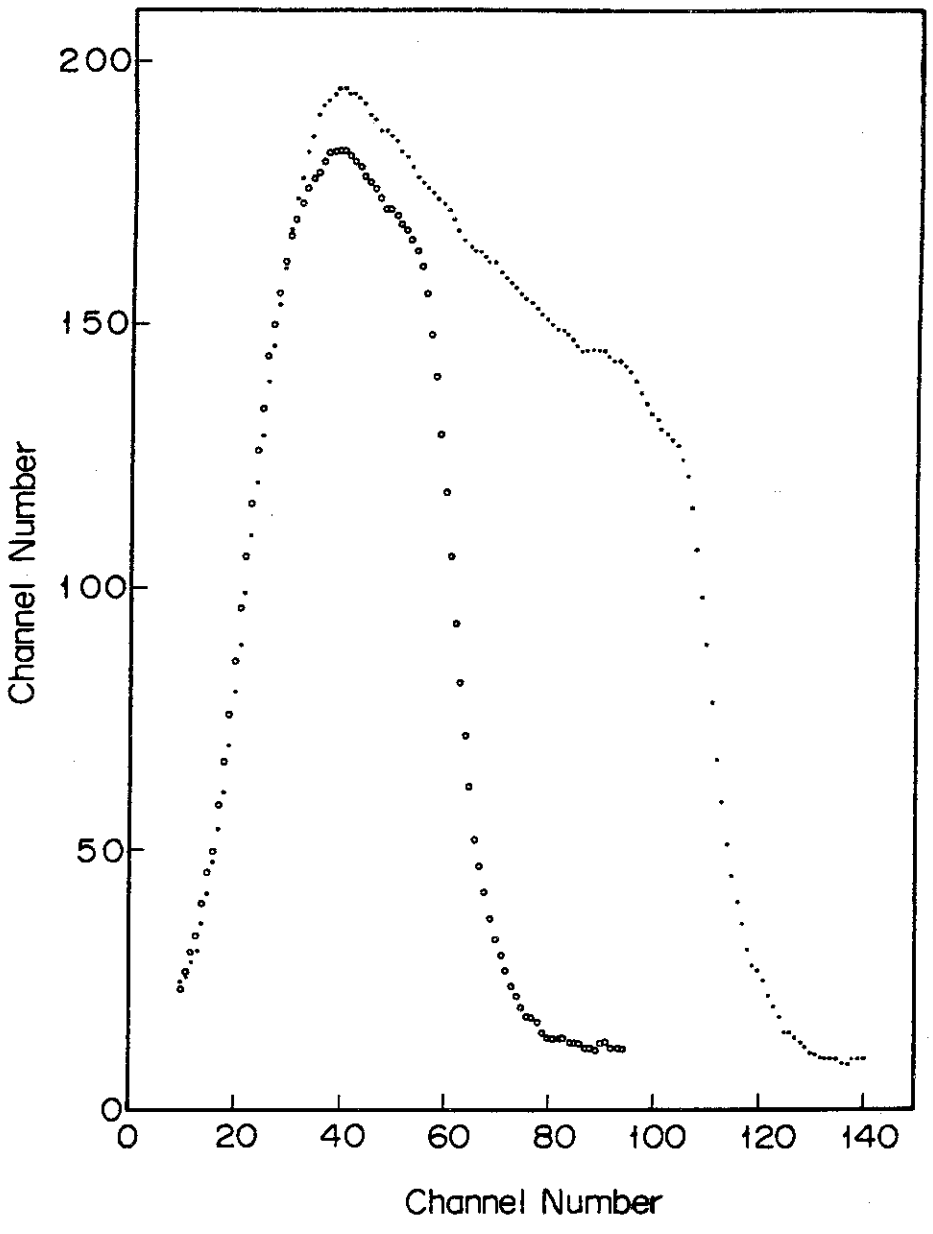


Fig. 9 Digitized Bragg curves of the elastically scattered $^{35}Cl$ from the Au target. The Bragg curves of the 129.8 MeV $^{35}Cl$ (dotted line) and of the 79 MeV $^{35}Cl$ (open circle) were digitized with the LeCroy waveform digitizer.